BMC Musculoskeletal Disorders

RESEARCH

Open Access

High molecular weight hyaluronic acid alleviates ovariectomy-induced bone loss in mice

Khangarid Tenger[1†], Keiichiro Komori[2†], Ami Maehara[2], Kyosuke Miyazaki[3], Eriko Marukawa[1,4], Toshitaka Yoshii[5] and Kunikazu Tsuji[5*]

Abstract

Background The rapid decline in ovarian function associated with menopause promotes osteoclast differentiation and increases bone resorption, disrupting of bone homeostasis and increasing the risk of osteoporosis. Hyaluronic acid (HA) is a polysaccharide ubiquitously present in the connective tissues. Recent reports indicate that high-molecular-weight HA (HMW-HA) promotes osteoblast proliferation, enhances alkaline phosphatase activity and mineral deposition, and promotes the expression of bone differentiation markers, such as Runx2 and osteocalcin. HMW-HA also inhibits the expression of the receptor activator of nuclear factor kappa-B ligand (RANKL) in osteoblasts. These results suggest that HMW-HA may be an effective therapeutic agent against postmenopausal osteoporosis. Therefore, this study aimed to examine whether HMW-HA alleviates ovariectomy (OVX)-induced bone loss in mice.

Methods Eight-week-old female C57BL/6 J mice were randomly divided into the following five groups: Group 1: Sham/saline, Group 2: OVX/saline, Group 3: OVX/HMW-HA [15 mg/kg]; Group 4: OVX/HMW-HA [30 mg/kg]; and Group 5: OVX/HMW-HA [60 mg/kg]. Mice were administered HMW-HA or saline subcutaneously starting from 1 week after OVX and changes in bone mass were analyzed at 5 weeks using three-dimensional micro-computed tomography (3D-μCT). In addition, changes in osteoclast parameters were analyzed histologically.

Results The reduction in trabecular bone volume and trabecular number was significantly ameliorated in the OVX/HMW-HA group compared with that observed in the OVX/saline group, along with a significant inhibition of the increase in trabecular spacing. In addition, the OVX/HMW-HA group exhibited a significant reduction in osteoclast surface area and number compared with the OVX/saline group, with no significant differences compared with the sham group. In vitro experiments revealed that depletion of HMW-HA from the culture medium by hyaluronidase treatment increased RANKL expression in the bone marrow stromal cell line ST2. These data suggest that HMW-HA alleviates OVX-induced bone loss by downregulating osteoclast formation and/or activity in mice.

Conclusion HMW-HA is a potential novel therapeutic agent for osteoporosis.

Keywords Hyaluronic acid, Osteoporosis, Ovariectomy, Receptor activator of nuclear factor kappa-B ligand

[†]Khangarid Tenger and Keiichiro Komori contributed equally to this work.

*Correspondence:
Kunikazu Tsuji
tsuji.orj@tmd.ac.jp
Full list of author information is available at the end of the article

Background

Osteoporosis is a skeletal disorder characterized by reduced bone mass and strength, which increase fracture risk. Osteoporosis is regarded as a major health concern, particularly in aging populations, owing to its typically extended course and the rapid decline in activities of daily living associated with fractures, frailty, and osteoarthritis [1]. Thus, the clinical implications and economic impact of this disorder underscore the need to identify individuals at an elevated risk to facilitate timely and appropriate therapeutic interventions. Menopause is caused by a decline in ovarian function, and is a major risk factor for osteoporosis. An estimated 200 million women worldwide are diagnosed with osteoporosis, with approximately one-third of women aged 50 and older experiencing fragility fractures [2].

Osteoporosis is associated with abnormally elevated bone turnover, with osteoclast-mediated bone resorption exceeding osteoblast-mediated bone formation. Therapeutic strategies have focused on pharmacological interventions to rebalance bone metabolism by either stimulating osteoblastic bone formation or inhibiting osteoclast-mediated bone resorption. Drugs that promote bone formation include calcitriol, a recombinant human parathyroid hormone analog, and anti-sclerostin monoclonal antibodies. Bone resorption inhibitors include bisphosphonates, anti-receptor activator of nuclear factor kappa-B ligand (RANKL) monoclonal antibodies, and selective estrogen receptor modulators. These drugs have shown excellent therapeutic effects; however, limitations and side effects associated with their use have been reported [3–8]. Considering the currently available therapeutic options, safer and more patient-friendly drugs for the treatment of osteoporosis are urgently needed.

Hyaluronic acid (HA) is a high-molecular-weight polysaccharide composed of repeating disaccharide units of D-glucuronic acid and N-acetyl-D-glucosamine with a maximum molecular weight of 2×10^7 Da. It is widely distributed in the extracellular matrix of tissues such as skin, blood, bone, cartilage, synovial fluid, and eyes. HA plays a primary role in regulating the fluid and electrolyte balance in the body and lubricating joints because of its high water-binding capacity and viscoelastic properties [9–11]. Recent studies revealed that HA functions as a signaling molecule in various cell types [11]. Both the quantity and the molecular size (length) of HA are important regulatory factors in signal transduction. HA metabolism is regulated by HA synthase (HAS) and the degradation enzyme hyaluronidase (Hyal). Under physiological conditions, high molecular weight HA (HMW-HA) synthesized by HAS binds to cell surface receptors such as CD44 and Toll-like receptors (TLR2 and TLR4) on mesenchymal and inflammatory cells, contributing to tissue homeostasis [12–14]. Under pathological conditions, such as tissue damage, Hyal metabolizes HA to smaller molecules. Low molecular weight HA (LMW-HA; molecular weight below several tens of thousands of Da) functions as a damage-associated molecular patterns molecule and induces various inflammatory responses in inflammatory cells via TLR2 and TLR4 [13, 15, 16]. Thus, HA synthesis and metabolism are essential regulatory factors in tissue development and homeostasis.

HA has been shown to play an essential physiological role in the development and homeostasis of skeletal tissues. Mice lacking HAS2 in their limbs (*Has2$^{f/f}$;Prx1::cre*) exhibited shortening of long bones, patterning abnormalities of the phalanges, and joint formation defects. Conversely, mice lacking Hyal2 or cell migration-inducing protein exhibit bone formation abnormalities in the head and limbs, respectively [17–19]. In vitro studies have reported that HMW-HA enhances the expression of bone differentiation marker genes induced by bone morphogenetic protein-2 (BMP2) in osteoblast cell lines and negatively regulates RANKL expression in bone marrow stromal cells [20, 21].

Based on this information, we hypothesized that HMW-HA may play a physiological role in rebalancing bone metabolism and could be developed as an ideal new drug for osteoporosis treatment, possessing the ability to inhibit osteoclast-mediated bone resorption and promote osteoblast-mediated bone formation in vivo. To test this hypothesis and examine whether HMW-HA could be a new drug target for osteoporosis treatment, we administered HMW-HA subcutaneously to ovariectomized (OVX) mice and performed bone histomorphometric analysis. In this study, we demonstrated that HMW-HA effectively protected mice from OVX-induced bone loss. We expect this compound to be an ideal drug target for osteoporosis treatment because it has already been used for the treatment of osteoarthritis and is known to have a very low incidence of adverse effects.

Methods

Ethics

This study was approved by the Institutional Animal Care and Use Committee of the Tokyo Medical and Dental University (Approval Number: A2023-203A; Institute of Science Tokyo).

Materials

HMW-HA (cat#FCH-200: molecular weight $1.8\sim2.2\times10^6$ Da), which is fermented from *Streptococcus zooepidemicus*, was purchased from Kikkoman Biochemifa Company (Tokyo, Japan). Paraformaldehyde (PFA), ethylenediaminetetraacetic acid disodium salt

(cat#E5134: EDTA 2Na), tetrasodium salt (cat#ED4SS: EDTA 4Na), dexamethasone (cat#047–18863: DEX), and methyl green solution (cat#138–12,701) were purchased from Wako Pure Chemical Industries (Osaka, Japan). Toluidine Blue (cat#89,640), Leukocyte Acid Phosphatase (TRAP) (cat#387A-1KT), 1,25-dihydroxy vitamin D_3 (cat#D1530: $1,25(OH)_2D_3$) and hyaluronidase (cat#H-2251) were purchased from Sigma-Aldrich (St. Louis, MO, USA). Citric acid buffer (cat. #S236984-2) was purchased from Dako Agilent Technologies (Tokyo, Japan). Vectastain® Elite® ABC-HRP kit, (cat#PK-6101) was purchased from Vector Laboratories (Newark, CA, USA). Rabbit anti-mouse RANKL polyclonal antibody (cat#GTX32834) was purchased from Funakoshi (Tokyo, Japan). The 3,3′-diaminobenzidine tetrahydrochloride salt (DAB) Substrate (cat#MK210) was purchased from Takara Bio Incorporated (Shiga, Japan). The murine bone marrow stromal cell line ST2 (cat#RCB0224) was purchased from Riken Cell Bank (Ibaraki, Japan). RPMI-1640 (cat#30,264–85) medium and RPMI-1640 (cat#06261–65: phenol red-free) media were purchased from Nacalai Tesque Inc. (Kyoto, Japan). Fetal bovine serum (cat#12,483–020: FBS) and antibiotic–antimycotic (cat. #15,240,062) antibodies were purchased from Thermo Fisher Scientific (Waltham, MA, USA). Charcoal-stripped FBS was purchased from Serana Europe GmbH (Brandenburg, Germany). NucleoSpin® RNA (cat#740,955.50) was purchased from Macherey–Nagel Company (Duren, Germany). ReverTra Ace® qPCR RT Master Mix (cat#FSQ-201) and THUNDERBIRD® Next SYBR™ qPCR Mix (cat#QPX-201) were purchased from Toyobo Company (Osaka, Japan).

Ovariectomy

Eight-week-old female C57BL/6 J mice were purchased from Oriental Yeast Company (Tokyo, Japan). All mice were kept in a temperature- and humidity-controlled facility with a 12-h light/dark cycle and access to food and water ad libitum. After one week of acclimatization, the mice were randomly divided into five groups: Group 1: Sham surgery with saline injections (Sham/saline; $n=8$); Group 2: OVX with saline injections (OVX/saline; $n=8$); Group 3: OVX with HMW-HA injections (OVX/HMW-HA [15 mg/kg]; $n=8$); Group 4: OVX with HMW-HA injections (OVX/HMW-HA [30 mg/kg]; $n=8$); and Group 5: OVX with HMW-HA injections (OVX/HMW-HA [60 mg/kg]; $n=8$). Ovariectomies were performed using a double dorsolateral approach [22]. Briefly, the mice were placed under anesthesia with 2% isoflurane inhalation and the coat hair on the lumbar region was removed using clippers. The skin was disinfected with propidium iodide and vertical incisions were made on both dorsal sides of the lumbar region to expose the ovaries. After suturing the fallopian tubes, the ovaries were excised and the skin was sutured. The same surgical procedure was performed in the sham group, except for suturing of the fallopian tubes and removal of the ovaries. The mice were maintained at 37 °C until they recovered from anesthesia and were monitored frequently for 1 week post-surgery to ensure the absence of persistent bleeding or infection at the surgical site. No postoperative complications were observed in any mouse used in this study. One week after surgery, either HMW-HA or saline (0.5 mL) was injected subcutaneously into the dorsal aspect of the neck. The mice were euthanized by carbon dioxide inhalation at the end of the 5th week. The uteri were collected and weighed, and the femurs were dissected and analyzed for changes in bone metabolism by micro-computed tomography (μCT) and histology (Fig. 1A-B).

Three dimensional-μCT analysis

The right femurs from each group were morphometrically analyzed. Specimens were fixed in 70% ethanol for 2 weeks at 4 °C followed by acquisition of three-dimensional micro-computed tomography (3D-μCT) images using the Scan-Xmate-E090 (Comscan Techno, Kanagawa, Japan). Trabecular bone morphometric parameters, such as bone volume/tissue volume (BV/TV [%]), trabecular thickness (Tb.Th [μm]) trabecular number (Tb.N [1/mm]), trabecular separation (Tb.Sp [μm]) and trabecular connectivity density (Conn.D [$1/mm^3$]) [23], were analyzed in the metaphyseal region of the distal femur using Tri/3D-Bon-FCS64 software (Ratoc System Engineering, Tokyo, Japan). The region of interest (boxed in white in Fig. 2A) in the distal femur metaphysis was set 500 μm away from the growth plate (white line in Fig. 2A), with a thickness of 1000 μm.

Histological evaluations

The left femurs from each group were fixed in 4% PFA (pH 7.0) for 24 h and then kept in 70% ethanol solution at 4 °C for 2 weeks. The femurs were decalcified in 20% EDTA (pH 7.2) for 4 weeks, embedded in paraffin, and sagittal Sects. (8 μm in thickness) were prepared. Toluidine blue staining was performed for the histological analysis of the percentage of adipocytes per marrow volume (Ad.V/Ma.V [%]). Tartrate-resistant acidic phosphatase (TRAP) staining was conducted using a TRAP kit, according to the manufacturer's instructions. Bone resorption parameters, including osteoclast surface/bone surface (Oc.S/BS [%]) and osteoclast number/bone surface (N.Oc/BS [1/mm]) were analyzed according to guidelines published by the American Society for Bone and Mineral Research [24]. Osteoclast parameters were evaluated at two different positions in the distal femur

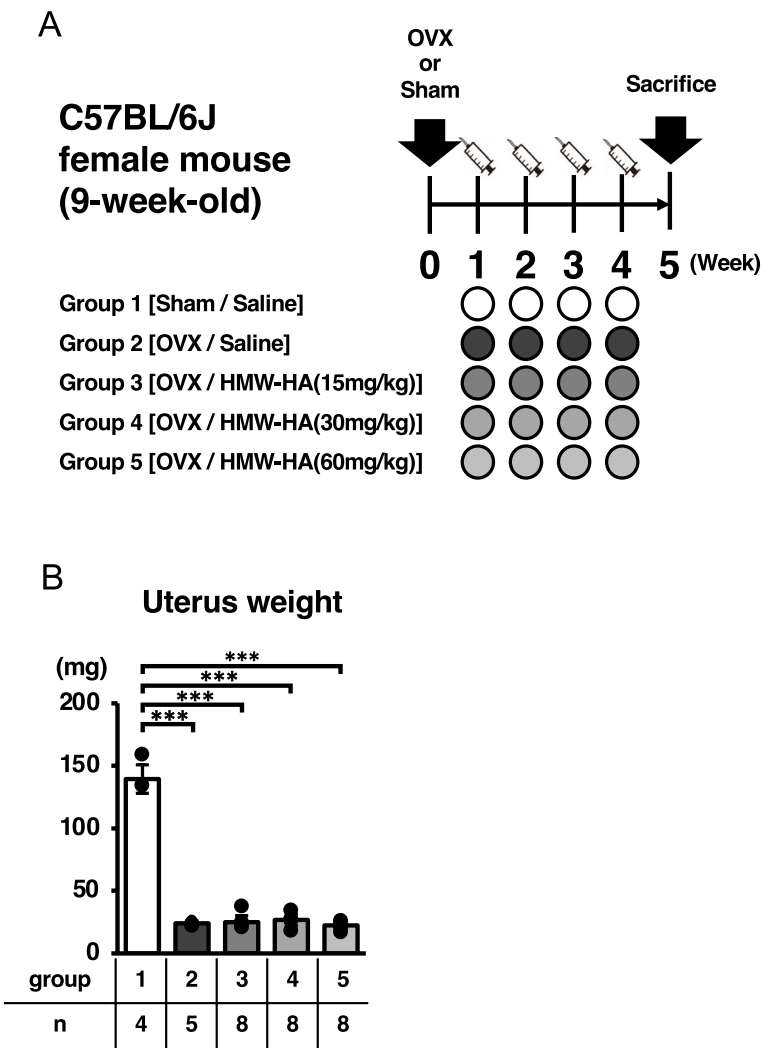

Fig. 1 Experimental design. **A** After sham or OVX surgery, 0.5 mL of either saline or each dose of HMW-HA were subcutaneously injected once a week. Mice were euthanized in the 5th week and femurs were analyzed. **B** Uterine weights of each group at week 5 are presented. Data are expressed as mean ± SD, analyzed by ANOVA followed by Tukey's post hoc test, showing all data points. *$p < 0.05$, ** $p < 0.01$, *** $p < 0.001$. The numbers of samples measured are indicated in the figure and in Supplementary Table 1

(mid-sagittal and peak of the lateral condyle). The region of interest (boxed in yellow in Fig. 3A and 4A) in the distal femur metaphysis was set 500 μm away from the growth plate (red line in Fig. 3A and 4A), with a thickness of 1000 μm. Calculations were performed using a Biorevo BZ-II Analyzer (Keyence, Osaka, Japan).

Immunohistochemical evaluations

For RANKL staining, antigens were retrieved using citric acid buffer (pH 6.0) at room temperature for 2 h. Sections were treated with 3% H_2O_2 to block endogenous peroxidases and incubated at room temperature for 1 h with blocking serum (Vectastain® Elite® ABC-HRP kit). Sections were then incubated with rabbit anti-mouse RANKL polyclonal antibody (1:200) at 4°C overnight. For visualization, Vectastain Elite ABC Reagent (Vectastain® Elite® ABC-HRP kit) and DAB staining were used according to the manufacturer's instructions. Secondary antibody incubation was performed at room temperature for 1 h. The nuclei were counterstained with methyl green. RANKL-positive osteocyte number/total osteocyte number × 100 ($Rankl^+$ osteocyte %) values were computed as described previously [25]. The region of interest (boxed in green in Fig. 3D) in the distal femur metaphysis was set 500 μm away from the growth plate (red line in Fig. 3D), with a thickness of 1000 μm. All images were acquired using a microscope (Biorevo BZ-9000; Keyence, Osaka, Japan). The $Rankl^+$

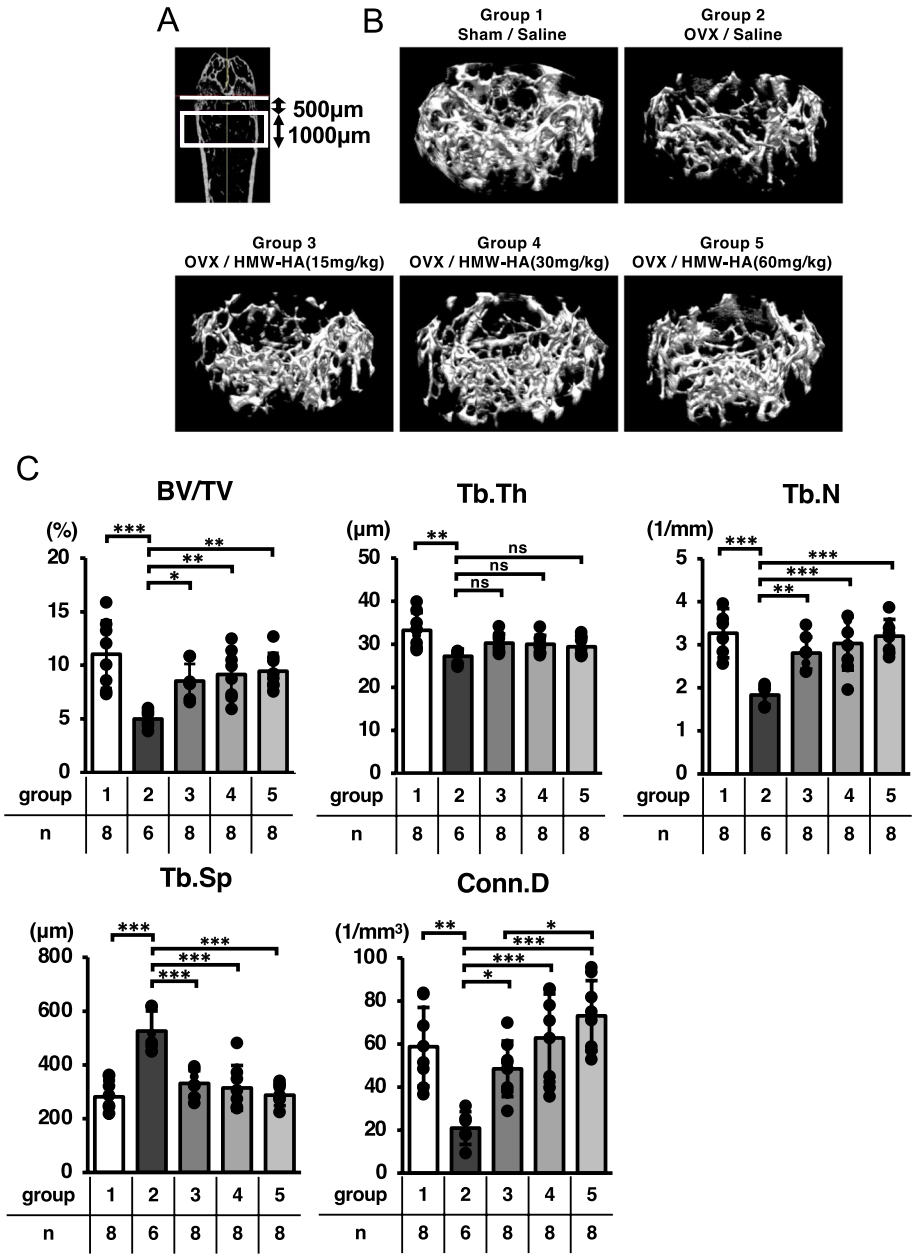

Fig. 2 HMW-HA reversed OVX-mediated bone loss. **A** The area computed by 3D-μCT analysis is indicated in the box in white. **B** Representative 3D μCT images of trabecular bone microarchitecture in the distal femurs of each group are indicated. **C** Bone volume (BV/TV), trabecular thickness (Tb. Th), number (Tb. N), separation (Tb. Sp) and connectivity density (Conn. D). Data are expressed as mean ± SD, analyzed by ANOVA followed by Tukey's post hoc test, showing all data points. *$p < 0.05$, ** $p < 0.01$, *** $p < 0.001$. ns, not significant. The number of samples are indicated at the bottom of each figure and in Supplementary Table 2

osteocyte % value was measured by two independent researchers who were blinded to the sample identity, and the Intraclass Correlation Coefficient (ICC) (2,1) was 0.804. As an experimental control, a negative control (without using a primary antibody) was also incorporated into the analysis; representative images are shown in Supplementary Fig. 1.

Cell culture

ST2 cells were maintained in complete growth medium (RPMI-1640) supplemented with 10% FBS, 1% Antibiotic–Antimycotic at 37 °C under an atmosphere of 5% CO_2. To examine the effects of HA signaling on the regulation of RANKL expression, 3×10^5 cells were seeded onto 35 mm diameter dishes and incubated in

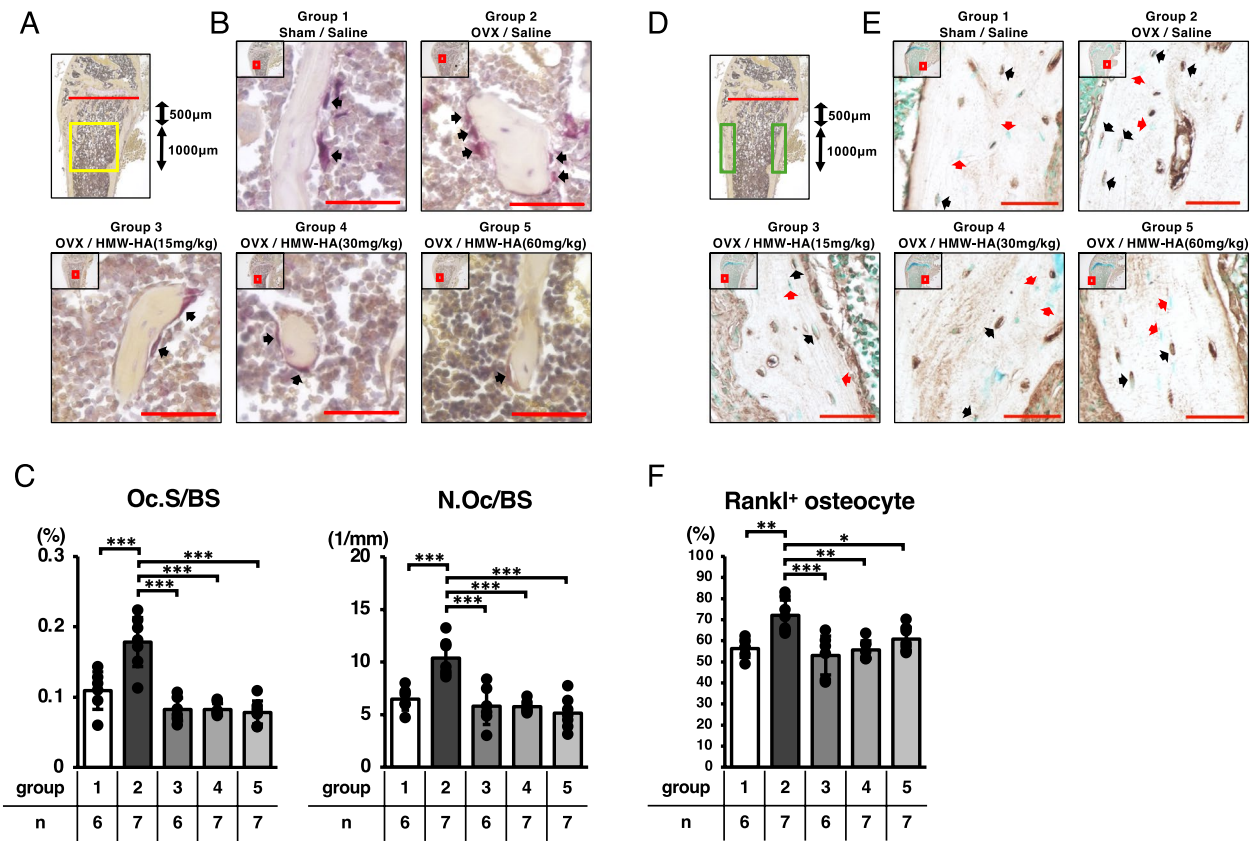

Fig. 3 HMW-HA downregulated osteoclastic bone resorption in ovariectomized mice through the downregulation of RANKL-expressing osteocytes. **A** The area analyzed for osteoclast parameters is indicated in the box in yellow. **B** Representative images of TRAP staining. Low-power images boxed in red are enlarged and presented in each panel. Black arrows indicate osteoclasts. Red bars in high-power images indicate scale bars (50 μm). **C** Bone resorption parameters including osteoclast surface per bone surface (Oc.S/BS) and osteoclast number per bone surface (N.Oc/BS) of each sagittal section. **D** The area analyzed for Rankl^{+} osteocyte percentage is indicated in the box in green. **E** Representative images of RANKL-positive osteocyte lacunes. Low-power images boxed in red are enlarged and presented in each panel. Black arrows indicate RANKL-positive osteocyte lacunes. Red arrows indicate osteocytes with no RANKL expression. Red bars in high-power images indicate scale bars (50 μm). **F** The Rankl.$^{+}$ osteocyte percentage was qualitatively assessed in each group. Data are expressed as mean ± SD, analyzed by ANOVA followed by Tukey's post hoc test, showing all data points. *$p < 0.05$, ** $p < 0.01$, *** $p < 0.001$. The number of samples are indicated at the bottom of each figure and in Supplementary Tables 3 and 4

complete growth medium for 12 h. To deplete the estrogen signal and induce osteoblastic differentiation, cells were incubated in RPMI-1640 (phenol red-free) supplemented with 10% charcoal-stripped FBS, 10^{-7} M DEX, and 10^{-7} M $1,25(OH)_2D_3$ in the presence or absence of 100 nM Hyal for 12 or 24 h.

Quantitative Reverse Transcriptase-Polymerase Chain Reaction (qRT-PCR)

Total RNA was isolated using the NucleoSpin® RNA according to the manufacturer's instructions. Complementary DNA was prepared with the ReverTra Ace® qPCR RT Master Mix. Quantitative RT-PCR (qRT-PCR) was conducted using THUNDERBIRD® Next SYBR™ qPCR Mix with the following specific primer sequences:

GAPDH, 5′ -GACGGCCGCATCTTCTTGA- 3′ (forward) and
5′ -CACACCGACCTTCACCATTTT- 3′ (reverse);
RANKL, 5′-TGGAAGGCTCATGGTTGGATG- 3′ (forward) and
5′ -AGTGACTTTATGGGAACCCGA - 3′ (reverse);
OPG, 5′ -ACTTGAAACGGCCCAGTGAT- 3′ (forward) and
5′ -ACTCAGAGTCCCCAGTGTGT- 3′ (reverse).

Thermal cycling and fluorescence detection were carried out using a LightCycler® 480 II /96 (Roche, Switzerland). The RANKL and OPG mRNA copy number values of each sample were normalized using primers specific for GAPDH mRNA, and relative expression levels were calculated using the $2^{-\Delta\Delta Ct}$ method [26]. The ratio of

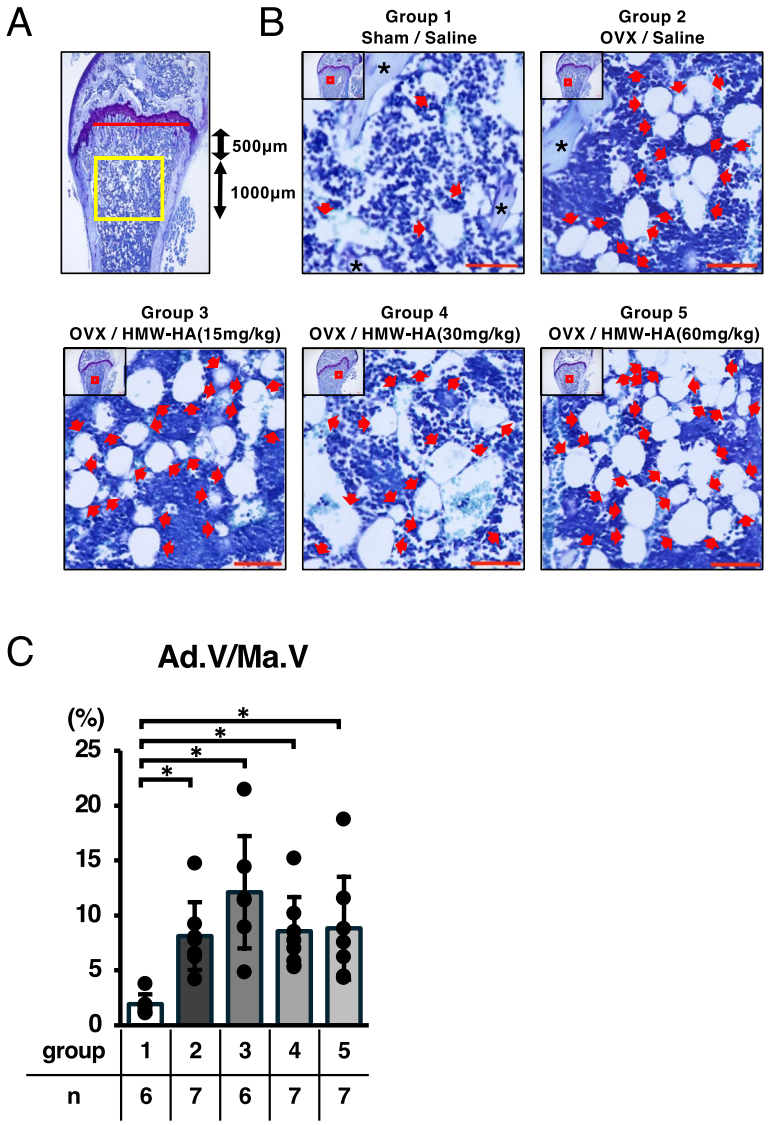

Fig. 4 HMW-HA had subtle effects on fatty marrow formation induced by OVX. **A** The area analyzed for percentage of adipocyte volume per marrow volume (Ad.V/Ma.V) is indicated in the box in yellow. **B** Representative images of the distal femur (toluidine blue staining). Low-power images boxed in red are enlarged and presented in each panel. Red arrows indicate cells with fat droplets. Black asterisks point to trabecular bone. Red scale bar = 50 μm. **C** Ad.V/Ma.V was calculated and plotted. Data are expressed as mean ± SD, analyzed by Kruskal–Wallis test followed by Steel–Dwass post hoc test, showing all data points. *$p < 0.05$. ns, not significant. Numerical data are presented in Supplementary Table 5

RANKL mRNA to OPG mRNA was calculated using the same method, in which the Ct value of RANKL was normalized to that of OPG.

Statistical analysis

Easy R (EZR version 1.63) was used for statistical evaluation [27]. To compare the differences in the parameters of bone structure, osteoclasts, and Rankl$^+$ osteocyte percentages, one-way analysis of variance followed by Tukey's post hoc test was carried out between the five groups (Sham/saline, OVX/saline, and OVX/HMW-HA groups). Adipocyte volume was analyzed using the Kruskal–Wallis test, followed by the Steel–Dwass post hoc test. The Wilcoxon signed-rank test was used to assess RANKL and OPG expression in ST2 cells. The Wilcoxon rank-sum test was used to assess the ratio of RANKL to OPG mRNA in ST2 cells. All data are expressed as the mean ± standard deviation (SD) and are presented in Supplemental Tables 1–6. Statistical significance was set at < 5% (*; $p < 0.05$).

Results

HMW-HA inhibited ovariectomy-induced bone loss in mice

HMW-HA was subcutaneously injected once per week into OVX mice to examine its pharmacological effects on bone metabolism (Fig. 1A). As indicated in Fig. 1B, uterine weights were significantly reduced in mice at 5 weeks post-ovariectomy (Sham/saline vs. OVX/saline or OVX/HMW-HA groups) (Fig. 1B, Table S1), indicating that ovarian function was successfully abolished in these mice, while 3D-μCT analyses indicated that trabecular bone volume in the metaphyseal region of the distal femur (BV/TV) was significantly reduced in the OVX/saline group compared with that in the Sham/saline group (Groups 1 and 2, Fig. 2B and C). Furthermore, morphometric analyses indicated significant reductions in trabecular thickness (Tb.Th), trabecular number (Tb.N), and trabecular connectivity (Conn.D), whereas trabecular separation (Tb.Sp) was significantly increased in the OVX/saline group (compare groups 1 and 2; Fig. 2C and Table S2). Weekly subcutaneous injections of HMW-HA reversed the ovariectomy-induced bone loss, although we observed no dose-dependent effects in the tested concentration range of HMW-HA (Fig. 2C, BV/TV, compare group 2 with groups 3–5). Detailed morphological analysis indicated that all trabecular bone parameters (Tb.Th., Tb.N., Conn.D., and Tb.Sp.) were restored to the levels observed in the sham/saline group (Fig. 2C and Table S2).

HMW-HA downregulated osteoclastic bone resorption in ovariectomized mice through the downregulation of RANKL-expressing osteocytes

Since 3D-μCT analyses indicated that subcutaneous injection of HMW-HA effectively reversed ovariectomy-induced bone loss, we analyzed the changes in trabecular bone resorption parameters in the metaphyseal trabecular area after HMW-HA injection. Histological analyses indicated that ovariectomy significantly increased both the number of osteoclasts per unit trabecular bone surface area (N.Oc/BS) and the osteoclast surface area per unit trabecular bone surface area (Oc.S/BS) in the metaphyseal region of the distal femur (compare groups 1 and 2 in Fig. 3B and C). Weekly subcutaneous injections of HMW-HA completely restored these parameters to control levels, although no dose-dependent effects were observed in the tested concentration range of HMW-HA (Fig. 3C and Table S3).

Previous studies have reported that osteocytes are the major source of RANKL. Therefore, we analyzed RANKL-expressing osteocytes in the cortical area of the metaphyseal region of the distal femur. As indicated in Figs. 3E and F, the ratio of RANKL-expressing osteocytes per unit cortical bone area was significantly increased in the ovariectomized mice (compare groups 1 and 2 in Fig. 3F). In parallel with the results of the osteoclast parameters, the subcutaneous injection of HMW-HA significantly reduced the ratio of RANKL-expressing osteocytes per unit of cortical bone area to the same levels as those observed in the sham/saline group, although no dose-dependent effects were observed in the tested concentration range of HMW-HA (Fig. 3F and Table S4).

The pharmacological effects of HMW-HA were not observed in relation to fat marrow changes associated with ovariectomy

Previous studies have reported that a decline in ovarian function leads to the progressive formation of fat marrow, which is associated with a decrease in bone formation capacity in postmenopausal osteoporosis. Thus, we analyzed the morphological changes in the bone marrow after HMW-HA injection in ovariectomized mice. Histological analyses indicated that ovariectomy induced fat marrow formation (Fig. 4B and C, comparing groups 1 and 2; arrows indicate adipocytes in the bone marrow region). However, we did not observe any inhibitory effect on fat marrow formation associated with the subcutaneous injection of any dose of HMW-HA after ovariectomy (Fig. 4B, C, and Supplementary Table S5; arrows indicate adipocytes in the bone marrow region).

HA negatively regulates RANKL expression in mouse bone marrow stroma-derived ST2 cells

Histological and immunohistochemical analyses suggested that HMW-HA suppresses osteoclast-mediated bone resorption by downregulating RANKL expression in osteoblasts and osteocytes. To test this hypothesis, we evaluated the mRNA expression of RANKL and OPG mRNA expression levels and their regulation by HMW-HA in ST2 cells. ST2 cells are derived from bone marrow stromal cells and can differentiate into osteoblasts in vitro in the presence of $1,25(OH)_2D_3$ and DEX. After incubating the ST2 cells for 12 h to allow adherence to the dish, they were incubated in charcoal-stripped FBS with $1,25(OH)_2D_3$ and DEX for 12 or 24 h, and RANKL and OPG mRNA expression levels were quantified by qRT-PCR. Because FBS contains HMW-HA, we removed it from the medium with Hyal instead of supplementing it to investigate its effects on RANKL and OPG expression in ST2 cells (Fig. 5A). As shown in Fig. 5B and Supplementary Table S6, the removal of HMW-HA from the culture medium significantly increased RANKL and OPG mRNA expression in ST2 cells at 12 h. RANKL mRNA expression continued to increase, whereas no statistically significant difference in OPG mRNA expression was observed at 24 h (Fig. 5C and Supplementary Table S6). As a result,

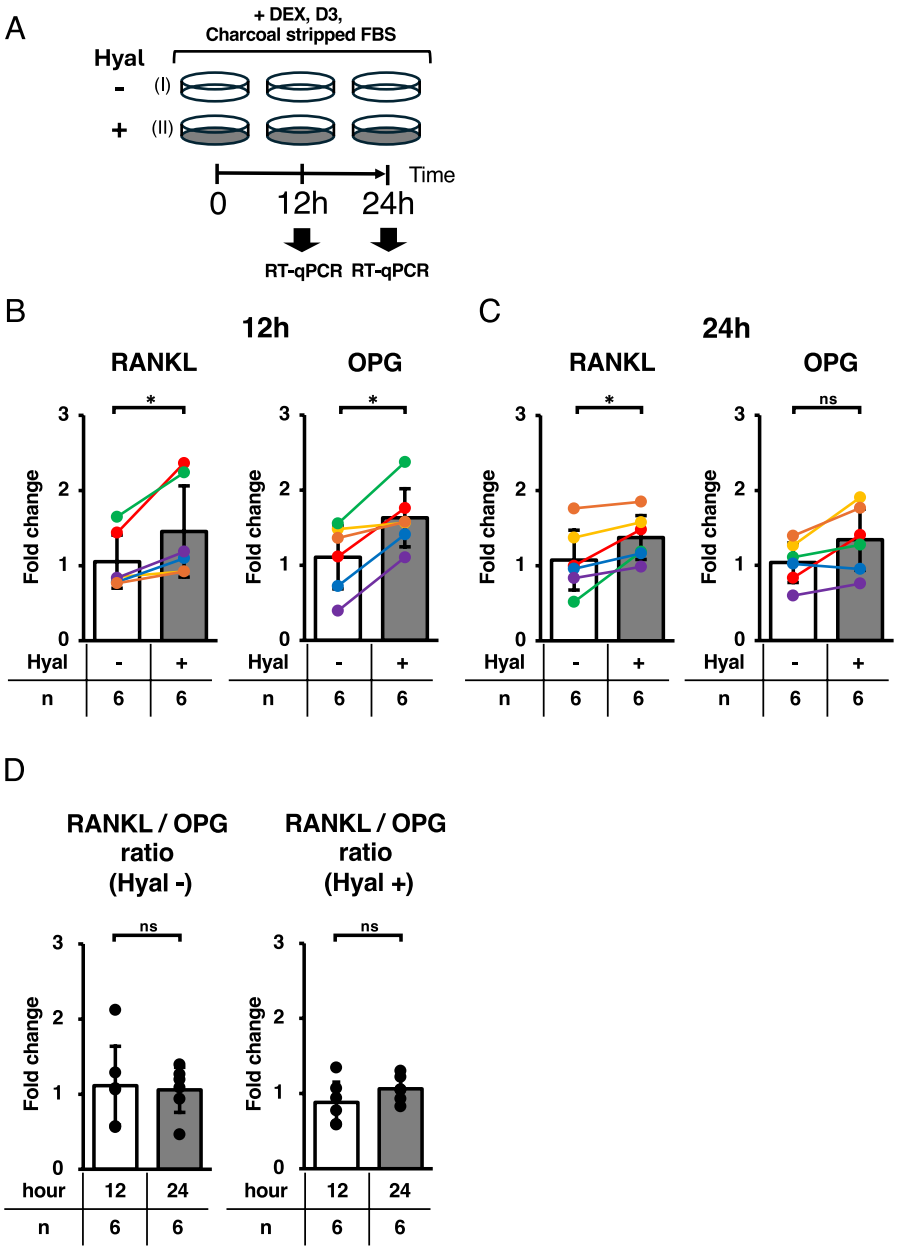

Fig. 5 Removal of HMW-HA from estrogen-deficient culture medium increased the RANKL expression in ST2 cells. **A** Experimental plan. Three hundred thousand cells were incubated for 12 h in RPMI-1640 medium. After cells were attached to the dishes, culture media were replaced with (I) charcoal-stripped FBS and (II) charcoal-stripped FBS with 100 nM of hyaluronidase for 12 h or 24 h. **B**, **C** Relative expression of RANKL and OPG in the presence or absence of hyaluronidase at 12 and 24 h. Colorful lines are associated with each 12 and 24 h samples. **D** Average ratio of RANKL mRNA to OPG mRNA in the presence or absence of hyaluronidase. Data are expressed as mean ± SD, analyzed by Wilcoxon signed-rank test (**B**, **C**), Wilcoxon rank-sum test (**D**), showing all data points. *$p < 0.05$. ns, not significant. $n = 6$ per group. Numerical data are presented in Supplementary Table 6

the average ratio of RANKL mRNA to OPG mRNA increased with the incubation period in the Hyal-treated group, although the difference was not statistically significant (0.88 ± 0.27 at 12 h to 1.06 ± 0.16 at 24 h, Fig. 5D right panel and Supplementary Table S6). In contrast, the ratio did not alter in the control (Hyal-) group (1.11 ± 0.52 at 12 h to 1.06 ± 0.30 at 24 h, Fig. 5D left panel and Supplementary Table S6).

Discussion

Postmenopausal osteoporosis, resulting from estrogen deficiency, is the most common type of osteoporosis. Estrogen deficiency leads to increased osteoclast number and activity [28]. The imbalance in bone metabolism due to elevated bone resorption activity surpasses bone formation and has primary effects on trabecular bone morphology, such as loss of trabecular thickness, number, and connectivity [29]. In this study, we showed that subcutaneous injection of HMW-HA effectively inhibited ovariectomy-induced morphometric changes in mouse trabecular bones. These results suggest that HMW-HA plays a significant biological role in rebalancing bone metabolism. Because HMW-HA has already been clinically used as a treatment for osteoarthritis, its safety is ensured when administered to humans. In addition, HMW-HA has been shown to have a relatively low incidence of adverse effects during long-term intervention [30]. This could be attributed to its biochemical nature as a polysaccharide with low immunogenicity. Therefore, we expect HMW-HA to be a promising new candidate for the treatment of osteoporosis.

In this study, we showed that the pharmacological functions of HMW-HA may be mediated, at least in part, by the suppression of osteoclast development and activation via the downregulation of RANKL expression in osteocytes and osteoblasts. Osteocytes are a major source of RANKL in long bones [31]. Our immunohistochemical analyses indicated that HMW-HA restored the ratio of RANKL-expressing osteocytes to total osteocyte lacune numbers in femoral cortical bones to the same levels as those observed in the sham/saline group, while this ratio was significantly elevated in the OVX/saline group. We also showed that depletion of HMW-HA in the culture medium by Hyal treatment significantly upregulated RANKL mRNA expression in bone marrow stroma-derived ST2 cells. In contrast, upregulation of OPG mRNA expression was transient. The average ratio of RANKL mRNA to OPG mRNA increased during the incubation period in the absence of HMW-HA. These results suggest that serum HMW-HA may suppress the RANKL signaling pathway in bone.

Although the underlying molecular mechanisms have not been fully elucidated, both direct and indirect molecular mechanisms employed by HMW-HA to regulate bone mass may be considered. The direct effects of HMW-HA may be mediated via cell surface receptors, including CD44, TLR4, Receptor for Hyaluronan-mediated Mobility, Lymphatic vessel endothelial hyaluronan receptor-1, layilin, and stabilin/hyaluronic acid receptors for endocytosis. Among these, the signals activated by CD44 in mesenchymal cells have been reported to include the regulation of RANKL by HA [12, 32, 33].

Ariyoshi et al. reported that supplementing the culture medium with HMW-HA significantly suppresses RANKL expression in ST2 cells, whereas the addition of 4-MU, an HA synthesis inhibitor, upregulates it. They also showed that the suppression of RANKL expression by HMW-HA was reversed by the neutralizing antibody for CD44 and by the application of the RhoA GTPase inhibitors simvastatin and Y27632 [21]. Thus, one possible direct molecular mechanism by which HMW-HA may suppress RANKL involves the activation of the CD44-RhoA signaling axis in bone cells. However, contradictory experimental results have been reported. Cao et al. reported different findings from those of Ariyoshi et al. by showing that HMW-HA enhances RANKL expression in primary mouse bone marrow stromal cells (BMSCs) [34]. This effect was completely abolished in BMSCs derived from CD44 knockout mice. Furthermore, CD44 knockout mice showed elevated bone mass when compared with control mice. Cao et al. claimed that the HA-CD44 signaling axis positively regulates RANKL expression in the bone. Although our present data are in line with those reported by Ariyoshi et al., further careful analysis is warranted to fully elucidate the role of the HA-CD44 signaling axis in the regulation of RANKL expression in the bone.

TLR4 is another major receptor of HMW-HA. Chang et al. reported that HMW-HA inhibits osteoclast differentiation from bone marrow-derived macrophages via TLR4 [16]. They showed that HMW-HA suppresses RANK expression by downregulating the M-CSF-AP-1/MITF signaling pathway. These data suggest that the pharmacological action of HMW-HA may directly target osteoclast precursor cells.

Estrogen deficiency reportedly leads to increased serum IL-7 levels, which promote T cell activation. Activated T cells produce proinflammatory cytokines such as IL-1b, IL-6, and TNF-alpha [35, 36]. It is possible that HMW-HA indirectly inhibits RANKL expression through its anti-inflammatory function because these proinflammatory cytokines promote RANKL expression in bone cells. These findings clearly demonstrated the diverse pharmacological actions of HA in the regulation of bone resorption. Thus, it is crucial to identify the primary target cells of HA in bone to elucidate the overall molecular mechanism and assess the contributions of each action.

Both osteoclasts and osteoblasts have been shown to be targets of estrogen signaling in bone metabolism. Estrogen activates the Wnt/beta-catenin signaling pathway to increase osteogenesis [35]. Estrogen has also been reported to enhance BMP signaling and induce stromal cells to differentiate into osteoblasts rather than adipocytes [36]. Kawano et al. reported that HMW-HA also

enhanced osteoblastic differentiation induced by BMP2 in osteosarcoma-derived MG63 cells [20]. To probe the pharmacological effects of HA on osteogenesis, we evaluated whether HA inhibits the formation of fat marrow associated with OVX. Our findings suggest that the subcutaneous injection of HMW-HA does not inhibit the differentiation of bone marrow stromal cells into adipocytes. However, further investigation is required to fully understand the pharmacological effects of HA on osteogenesis.

In this study, we investigated three different concentrations of HMW-HA ranging from 15 to 60 mg/kg. These concentrations were estimated to correspond to 187.5 to 750 μg/mL in each mouse, assuming a mouse weight of 25 g and a total blood volume of 2 mL. These experimental conditions were determined based on concentrations used in previous in vitro studies investigating RANKL expression in bone cells [21]. However, we did not observe a concentration-dependent effect on bone mass recovery within the concentration range of HMW-HA tested in this study. Based on these findings, we believe that the pharmacological effects of HMW-HA can be achieved at lower dosages.

To the best of our knowledge, this is the first study to report that HMW-HA alleviates OVX-induced bone loss in mice. Recently, Kikuchi et al. reported that subcutaneous administration of HMW-HA (2.7 MDa) inhibited bone resorption and promoted bone formation in OVX rats [37]. Stancikova et al. showed that oral administration of HMW-HA (1.62 MDa) inhibited bone resorption in OVX rats [38]. The results of these studies are consistent with those of our study, and we anticipate that the pharmacological effects of HMW-HA may be conserved across species.

This study has several limitations and unresolved issues. First, we injected the HA solution 1 week after OVX. Thus, it remains unclear whether HMW-HA simply inhibits bone loss or if it improves bone metabolism by promoting bone formation in response to bone loss. Experiments to address this question should focus on the therapeutic administration of HMW-HA for bone loss following OVX, the measurement of bone morphometric parameters such as mineral apposition rate and bone formation rate, and the assessment of serum bone metabolism markers such as procollagen type I N-propeptide and tartrate-resistant acid phosphatase 5b. In addition, to substantiate the potential of this drug as a treatment for osteoporosis, it is essential to demonstrate not only an improvement in bone volume, but also a reduction in bone fragility and the prevention of fragility fractures. Therefore, the impact of HMW-HA treatment on the mechanical properties of bone must be evaluated. These unresolved questions are the highest priority in our next experimental plan. Second, the optimal concentration of HMWHA was not determined. Third, we did not consider the effects of post-injection HA metabolism and pharmacokinetics. Hyal degrades HA to LMW-HA, which has been reported to possess various physiological activities. Therefore, comparing the pharmacological effects of HMW- and LMW-HA and their pharmacokinetics is important issue to address. Fourth, HMW-HA was administered via subcutaneous injection. However, less burdensome methods of administration need to be explored, such as oral delivery, in a clinical setting. Animal studies have reported that HA with a molecular weight less than 10 kDa is absorbed from the intestinal tract and transported to the portal vein and thoracic lymph following oral administration. However, HA with a molecular weight of 300 kDa is barely absorbed [39]. The absorption efficiency and pharmacokinetics of the HMW-HA used in this study (2 MDa) were not tested for oral administration. Optimizing the intestinal absorption of orally administered HMW-HA may require the implementation of a sophisticated drug delivery system such as cholesterol-modified nanocarriers.

Conclusion

In conclusion, administration of HMW-HA effectively protected mice from ovariectomy-induced bone loss.

Abbreviations

RANKL	Receptor activator of nuclear factor kappa-B ligand
HA	Hyaluronic acid
HAS	Hyaluronic acid synthase
Hyal	Hyaluronidase
HMW-HA	High molecular weight hyaluronic acid
LMW-HA	Low molecular weight hyaluronic acid
TLR	Toll-like receptor
OVX	Ovariectomy
3D-μCT	Three-dimensional micro-computed tomography
BV/TV	Bone volume / Tissue volume
Tb.Th	Trabecular thickness
Tb.N	Trabecular number
Tb.Sp	Trabecular separation
Conn.D	Trabecular connectivity density
Oc.S/BS	Osteoclast surface / Bone surface
N.Oc/BS	Osteoclast number / Bone surface
ST2	Mouse bone marrow stromal cell line
RPMI-1640	Roswell park memorial institute 1640
FBS	Fetal bovine serum
DEX	Dexamethasone
1,25(OH)2D3	1,25-Dihydroxy-vitamin D_3
GAPDH	Glyceraldehyde 3-phosphate dehydrogenase
BMSC	Bone marrow stromal cell
RANK	Receptor activator of nuclear factor kappa-B
M-CSF	Macrophage colony stimulating factor
AP-1	Activator protein-1
MITF	Microphthalmia-associated transcription factor
IL	Interleukin
TNF	Tumor necrosis factor
BMP	Bone morphogenetic protein
SD	Standard deviation
Ad.V/Ma.V	Adipocyte volume / marrow volume
OPG	Osteoprotegerin

Supplementary Information

The online version contains supplementary material available at https://doi.org/10.1186/s12891-024-08161-y.

Supplementary Material 1.

Acknowledgements
The authors thank Ms. Namiko Katayama and Ms. Mayumi Tsukamoto for their administrative contribution. We would like to thank Editage (http://www.editage.com) for English language editing.

Authors' contributions
Substantial contributions to study conception and design: KT (Tenger), KK, AM, KM, KT (Tsuji) Substantial contributions to acquisition of data: KT (Tenger), KK, AM, KT (Tsuji) Substantial contributions to analysis and interpretation of data: KT (Tenger), KK, AM, KM, EM, TY, KT (Tsuji) Drafting the article or revising it critically for important intellectual content: KT (Tenger), KK, AM, KM, KT (Tsuji) All authors read and approved the final manuscript. Final approval of the version of the article to be published: KT (Tenger), KK, AM, KM, KT (Tsuji).

Funding
This study was supported by the Japan Society for the Promotion of Science (JSPS) for KT (grant numbers 21K09196 and 24K12325). This funding body was not involved in the design of the study; collection, analysis, and interpretation of the data; or writing of the manuscript.

Data availability
The datasets used and analyzed during the current study are available from the corresponding author on reasonable request.

Declarations

Ethics approval and consent to participate
This study was approved by the Institutional Animal Care and Use Committee of the Tokyo Medical and Dental University (Approval Number: A2023-203A; Institute of Science Tokyo). Clinical trial number: not applicable.

Competing interests
The authors declare no competing interests.

Author details
[1]Department of Regenerative and Reconstructive Dental Medicine, Graduate School of Medical and Dental Sciences, Tokyo Medical and Dental University (Institute of Science Tokyo), 1-5-45 Yushima Bunkyo-Ku, Tokyo 113-8519, Japan. [2]Department of Nano-Bioscience, Graduate School of Medical and Dental Sciences, Tokyo Medical and Dental University (Institute of Science Tokyo), 1-5-45 Yushima Bunkyo-Ku, Tokyo 113-8519, Japan. [3]NR Laboratory, 493-10 Komakidai Nagareyama, Chiba 270-0113, Japan. [4]Dental Implant Clinic, Tokyo Medical and Dental University Hospital (Institute of Science Tokyo Hospital), 1-5-45 Yushima Bunkyo-Ku, Tokyo 113-8519, Japan. [5]Department of Orthopaedic Surgery, Graduate School of Medical and Dental Sciences, Tokyo Medical and Dental University (Institute of Science Tokyo), 1-5-45 Yushima Bunkyo-Ku, Tokyo 113-8519, Japan.

Received: 16 October 2024 Accepted: 5 December 2024
Published online: 19 December 2024

References

1. Yong EL, Logan S. Menopausal osteoporosis: screening, prevention and treatment. Singapore Med J. 2021;62(4):159–66.
2. Kanis JA. Assessment of fracture risk and its application to screening for postmenopausal osteoporosis: synopsis of a WHO report. WHO Study Group Osteoporos Int. 1994;4(6):368–81.
3. Reid IR, Billington EO. Drug therapy for osteoporosis in older adults. Lancet. 2022;399(10329):1080–92.
4. Camacho PM, Petak SM, Binkley N, Diab DL, Eldeiry LS, Farooki A, Harris ST, Hurley DL, Kelly J, Lewiecki EM, et al. American Association Of Clinical Endocrinologists/American College Of Endocrinology Clinical Practice Guidelines For The Diagnosis And Treatment Of Postmenopausal Osteoporosis-2020 Update. Endocr Pract. 2020;26(Suppl 1):1–46.
5. Hanley DA, Adachi JD, Bell A, Brown V. Denosumab: mechanism of action and clinical outcomes. Int J Clin Pract. 2012;66(12):1139–46.
6. Baron R, Ferrari S, Russell RG. Denosumab and bisphosphonates: different mechanisms of action and effects. Bone. 2011;48(4):677–92.
7. Gennari L, Merlotti D, Nuti R. Selective estrogen receptor modulator (SERM) for the treatment of osteoporosis in postmenopausal women: focus on lasofoxifene. Clin Interv Aging. 2010;5:19–29.
8. Kishida K, Furukawa M, Nakashima M, Kubota I, Hayashi Y. Selective estrogen receptor modulators and deep venous thrombosis after an emergent operation in senior women. JA Clin Rep. 2023;9(1):73.
9. Neuman MG, Nanau RM, Oruña-Sanchez L, Coto G. Hyaluronic acid and wound healing. J Pharm Pharm Sci. 2015;18(1):53–60.
10. Marinho A, Nunes C, Reis S. Hyaluronic acid: a key ingredient in the therapy of inflammation. Biomolecules. 2021;11(10):1518.
11. Abatangelo G, Vindigni V, Avruscio G, Pandis L, Brun P. Hyaluronic acid: redefining its role. Cells. 2020;9(7):1743.
12. Kobayashi T, Chanmee T, Itano N. Hyaluronan: metabolism and function. Biomolecules. 2020;10(11):1525.
13. Avenoso A, D'Ascola A, Scuruchi M, Mandraffino G, Calatroni A, Saitta A, Campo S, Campo GM. Hyaluronan in experimental injured/inflamed cartilage: In vivo studies. Life Sci. 2018;193:132–40.
14. Altman RD, Dasa V, Takeuchi J. Review of the Mechanism of Action for Supartz FX in Knee Osteoarthritis. Cartilage. 2018;9(1):11–20.
15. Ferreira NDR, Sanz CK, Raybolt A, Pereira CM, DosSantos MF. Action of Hyaluronic Acid as a Damage-Associated Molecular Pattern Molecule and Its Function on the Treatment of Temporomandibular Disorders. Front Pain Res (Lausanne). 2022;3: 852249.
16. Chang EJ, Kim HJ, Ha J, Ryu J, Park KH, Kim UH, Lee ZH, Kim HM, Fisher DE, Kim HH. Hyaluronan inhibits osteoclast differentiation via Toll-like receptor 4. J Cell Sci. 2007;120(Pt 1):166–76.
17. Jadin L, Wu X, Ding H, Frost GI, Onclinx C, Triggs-Raine B, Flamion B. Skeletal and hematological anomalies in HYAL2-deficient mice: a second type of mucopolysaccharidosis IX? FASEB J. 2008;22(12):4316–26.
18. Matsumoto K, Li Y, Jakuba C, Sugiyama Y, Sayo T, Okuno M, Dealy CN, Toole BP, Takeda J, Yamaguchi Y, et al. Conditional inactivation of Has2 reveals a crucial role for hyaluronan in skeletal growth, patterning, chondrocyte maturation and joint formation in the developing limb. Development. 2009;136(16):2825–35.
19. Shimoda M, Yoshida H, Mizuno S, Hirozane T, Horiuchi K, Yoshino Y, Hara H, Kanai Y, Inoue S, Ishijima M, et al. Hyaluronan-Binding Protein Involved in Hyaluronan Depolymerization Controls Endochondral Ossification through Hyaluronan Metabolism. Am J Pathol. 2017;187(5):1162–76.
20. Kawano M, Ariyoshi W, Iwanaga K, Okinaga T, Habu M, Yoshioka I, Tominaga K, Nishihara T. Mechanism involved in enhancement of osteoblast differentiation by hyaluronic acid. Biochem Biophys Res Commun. 2011;405(4):575–80.
21. Ariyoshi W, Okinaga T, Knudson CB, Knudson W, Nishihara T. High molecular weight hyaluronic acid regulates osteoclast formation by inhibiting receptor activator of NF-κB ligand through Rho kinase. Osteoarthritis Cartilage. 2014;22(1):111–20.
22. Park SB, Lee YJ, Chung CK. Bone mineral density changes after ovariectomy in rats as an osteopenic model : stepwise description of double dorso-lateral approach. J Korean Neurosurg Soc. 2010;48(4):309–12.
23. Bouxsein ML, Boyd SK, Christiansen BA, Guldberg RE, Jepsen KJ, Müller R. Guidelines for assessment of bone microstructure in rodents using micro-computed tomography. J Bone Miner Res. 2010;25(7):1468–86.
24. Dempster DW, Compston JE, Drezner MK, Glorieux FH, Kanis JA, Malluche H, Meunier PJ, Ott SM, Recker RR, Parfitt AM. Standardized nomenclature, symbols, and units for bone histomorphometry: a 2012 update of the report of the ASBMR Histomorphometry Nomenclature Committee. J Bone Miner Res. 2013;28(1):2–17.
25. El Khassawna T, Merboth F, Malhan D, Böcker W, Daghma DES, Stoetzel S, Kern S, Hassan F, Rosenbaum D, Langenstein J, et al. Osteocyte Regulation of Receptor Activator of NF-κB Ligand/Osteoprotegerin in a Sheep Model of Osteoporosis. Am J Pathol. 2017;187(8):1686–99.

26. Niikura T, Hak DJ, Reddi AH. Global gene profiling reveals a downregulation of BMP gene expression in experimental atrophic nonunions compared to standard healing fractures. J Orthop Res. 2006;24(7):1463–71.
27. Kanda Y. Investigation of the freely available easy-to-use software "EZR" for medical statistics. Bone Marrow Transplant. 2013;48(3):452–8.
28. Walker MD, Shane E. Postmenopausal Osteoporosis. N Engl J Med. 2023;389(21):1979–91.
29. Barger-Lux MJ, Recker RR. Bone microstructure in osteoporosis: transilial biopsy and histomorphometry. Top Magn Reson Imaging. 2002;13(5):297–305.
30. Bannuru RR, Brodie CR, Sullivan MC, McAlindon TE. Safety of Repeated Injections of Sodium Hyaluronate (SUPARTZ) for Knee Osteoarthritis: A Systematic Review and Meta-Analysis. Cartilage. 2016;7(4):322–32.
31. Nakashima T, Hayashi M, Fukunaga T, Kurata K, Oh-Hora M, Feng JQ, Bonewald LF, Kodama T, Wutz A, Wagner EF, et al. Evidence for osteocyte regulation of bone homeostasis through RANKL expression. Nat Med. 2011;17(10):1231–4.
32. Hansen B, Longati P, Elvevold K, Nedredal GI, Schledzewski K, Olsen R, Falkowski M, Kzhyshkowska J, Carlsson F, Johansson S, et al. Stabilin-1 and stabilin-2 are both directed into the early endocytic pathway in hepatic sinusoidal endothelium via interactions with clathrin/AP-2, independent of ligand binding. Exp Cell Res. 2005;303(1):160–73.
33. Borowsky ML, Hynes RO. Layilin, a novel talin-binding transmembrane protein homologous with C-type lectins, is localized in membrane ruffles. J Cell Biol. 1998;143(2):429–42.
34. Cao JJ, Singleton PA, Majumdar S, Boudignon B, Burghardt A, Kurimoto P, Wronski TJ, Bourguignon LY, Halloran BP. Hyaluronan increases RANKL expression in bone marrow stromal cells through CD44. J Bone Miner Res. 2005;20(1):30–40.
35. Cheng CH, Chen LR, Chen KH. Osteoporosis due to hormone imbalance: an overview of the effects of estrogen deficiency and glucocorticoid overuse on bone turnover. Int J Mol Sci. 2022;23(3):1376.
36. Li J, Chen X, Lu L, Yu X. The relationship between bone marrow adipose tissue and bone metabolism in postmenopausal osteoporosis. Cytokine Growth Factor Rev. 2020;52:88–98.
37. Kikuchi T, Udagawa K, Sasazaki Y. High-molecular-weight Hyaluronan Administration Inhibits Bone Resorption and Promotes Bone Formation in Young-age Osteoporosis Rats. J Histochem Cytochem. 2024;72(6):373–85.
38. Stancíková M, Svík K, Istok R, Rovenský J, Velebný V. The effects of hyaluronan on bone resorption and bone mineral density in a rat model of estrogen deficiency-induced osteopenia. Int J Tissue React. 2004;26(1–2):9–16.
39. Sato Y, Joumura T, Takekuma Y, Sugawara M. Transfer of orally administered hyaluronan to the lymph. Eur J Pharm Biopharm. 2020;154:210–3.

Publisher's Note